The International Journal of Advanced Manufacturing Technology (2020) 111:2957–2970
https://doi.org/10.1007/s00170-020-06314-6

ORIGINAL ARTICLE

Parametric study of composite curved adhesive joints

J. M. C. Correia[1] · R. D. S. G. Campilho[1,2] · R. J. B. Rocha[1,2] · Y. Liu[3] · L. D. C. Ramalho[2]

Received: 8 April 2020 / Accepted: 26 October 2020 / Published online: 5 November 2020

Abstract
Nowadays, the adhesive bonding method has a very strong presence in the most varied industries, especially in aeronautics, which strongly boosted the use of adhesively bonded joints. Curved bonded joints are commonly used in the aeronautical industry, where curved panels typically made of carbon fibre-reinforced polymer (CFRP) are joined to fabricate several fuselage parts. This work compares the performance of three adhesives (brittle, moderately ductile and ductile) in curved single-lap joints (SLJ) bonded with CFRP adherends, considering the modifications of the following geometric parameters: overlap length (L_O), adherend thickness (t_P) and adherends' radius of curvature (R). For the analysis of these joints, the finite element method (FEM) was used with cohesive zone model (CZM), and the discussions of joint behaviour included the internal stresses of the adhesive, joint strength and energy dissipated at failure (U). Before the numerical analysis, validation with experiments was carried out considering flat SLJ, with positive results. The numerical study on the curved SLJ showed a significant maximum load (P_m) and U improvement by increasing L_O for the two ductile adhesives. For the same adhesives, bigger t_P reduced P_m. On the other hand, the brittle adhesive revealed to be only minor affected by these parameter variations. Thus, with this work, clear design guidelines are proposed for curved SLJ.

Keywords Adhesive joints · Curved joints · Composite material · Structural adhesives · Finite element method · Cohesive zone models

1 Introduction

Nowadays, adhesive bonding is a widely used technology in several industries, from the simplest ones like furniture or shoemaking to the high-tech ones such as aerospace and aeronautics. Actually, the aerospace industry was the major driving force for the acceptance of this novel technique. Most revolutionary in the use of composites on commercial liners is the Boeing 787, which contains 50% composite structures by weight and 90% by volume, and the Airbus A350XWB, with similar composite usage. In comparison, the Boeing 777, which entered service in 1995, contains only 10% of composite structures by weight [1]. Adhesively bonded joints present a number of benefits when compared with other joining methods such as riveting and welding [2, 3]. In fact, adhesive joining allows the possibility to join different materials and it preserves their integrity, since it does not require drilling neither it induces a heat-affected zone such as welding. Additionally, this technique provides more uniform stress distributions, good strength-weight and cost-effectiveness ratios, corrosion protection, flexible gap filing, vibration damping and improved aesthetics [4, 5]. Nonetheless, drawbacks of bonded joints include the requirement of a surface treatment prior to adhesive application, disassembly difficulties without damage, low resistance to temperature and humidity and joint design oriented towards the elimination of peel stresses [6]. For a widespread use of adhesively bonded joints, the structural behaviour prediction techniques, in terms of strength and failure modes, have been continuously improved. Nowadays, by applying the FEM, complex structures bonded with high ductile adhesives may be easily characterized. CZM is a powerful tool that, combined with the FEM, proved to be highly

✉ R. D. S. G. Campilho
raulcampilho@gmail.com

[1] Departamento de Engenharia Mecânica, Instituto Superior de Engenharia do Porto, Instituto Politécnico do Porto, Rua Dr. António Bernardino de Almeida, 431, 4200-072 Porto, Portugal

[2] INEGI – Pólo FEUP, Rua Dr. Roberto Frias, s/n, 4200-465 Porto, Portugal

[3] WMG, University of Warwick, Coventry CV4 7AL, UK

accurate for joints' strength prediction [7]. CZM was proposed 60 years ago [8, 9]. Ever since, several researchers improved and successfully applying this method to describe damage, dealing with the nonlinear zone ahead of the crack tip [10]. This model relies on traction-separation laws between stresses and relative displacements to simulate damage along pre-specified paths. The accuracy of this method requires an exact determination of the cohesive strengths in tension and in shear (t_n^0 and t_s^0, respectively), and the fracture toughness in mode I (G_{IC}) and mode II (G_{IIC}) [11].

A number of joint architectures is available for designers to choose the one suitable for the required application and load bearing. On the one hand, the SLJ is the most used, since it is the simplest to manufacture, and it is widely studied and skilled to stress the adhesive in its strongest direction. Even so, this architecture makes the adherends non-collinear, triggering significant through-thickness normal or peel (σ_y) stresses at the overlap ends [12]. On the other hand, the double-lap joint is slightly more difficult to produce, but it presents a balanced design, providing decreased bending moments, thus reducing σ_y and shear (τ_{xy}) stresses [13]. In addition, the scarf joint also presents manufacture constrains due to the required milling operation to build the taper angle. Nonetheless, it keeps the axis of loading in line with the joint, leading to transfer the loadings more efficiently, providing higher strength than the SLJ [14]. In realistic applications, since longitudinal lap joints in the fuselage structure are curved, but laboratory test specimens are flat, the effect of joint curvature should also be assessed. For example, Boeing's typical narrow body and wide body aeroplanes have a radius of curvature of 1.88 m and 3.23 m, respectively. It has been shown that the curved geometry plays an important role in the joint strength and damage tolerance, with emphasis to L_O, R and adhesive thickness (t_A) [15, 16]. The use of flat SLJ to size the curved joints for realistic structures introduces uncertainties, which may result in sub-optimal designs. Therefore, it is of significant importance to investigate the performance of the curved SLJ.

Few works are available in the literature addressing curved adhesive joints' behaviour. Ascione and Mancusi [17] evaluated the strength up to failure of curved joints as a function of R. An analytical model was proposed that accounts for the variable R, shear deformability and coupling effects between the axial and shear/flexure loadings. A numerical (FEM) approximation was also tested to study the effect of different joint parameters. The adherends of the studied joints were made of CFRP and carbon fibre-reinforced polymer (GFRP) embedded in a concrete/masonry matrix. The chosen R values were 1000, 2000 and 5000 mm, and infinite i.e. flat SLJ. It was concluded that R benefits the joint strength by delaying the energy absorption as the curvature radius decreases. Temiz et al. [18] experimentally studied the effect of arc length and R variations on the SLJ strength. Flat specimens (i.e. conventional SLJ) were used for benchmark purposes and curved joints with $R = 105$, 132 and 150 mm with steel adherends were manufactured. The authors concluded that the load bearing capacity of SLJ is enhanced when a curved overlap area is applied. In addition, it was observed that as R increases, the joints' load-carrying and displacement capabilities decrease, although presenting better performances than the flat SLJ. The study of Parida and Pradhan [19] numerically addressed the effects of induced delamination length and adherends' curvature on the strain energy release rates of SLJ. The joints were made with CFRP, and the width (B) was kept constant at 25 mm. The authors found that all modes of the strain energy release rates (G_I, G_{II} and G_{III} for tension, shear and tearing) of a curved joint with a previously embedded delamination at the interface between the first and second plies increase with the reduction of R. Moreover, the joints made with flatter adherends have higher resistance to delamination damage growth than those with higher adherends' curvature. This outcome contradicts other available studies. However, one may point as probable cause the pre-induced delamination that grows faster in a curved joint, rather than in a flat joint. Sato [20] analytically predicted the residual stresses of curved joints bonded with viscoelastic adhesives using the Dillard's models [21]. The disadvantage of the method is the limitation of applicability, since it can only be applied to long joints. The authors proposed a governing equation of a model in which the adherends are beams and the adhesive is a viscoelastic material, providing the distribution of a normal stress perpendicular to the interface between the adhesive and the adherends. Recently, Liu et al. [16] performed a CZM parametric study focused on the effect of the size, curvature and free edges on the strength prediction of CFRP joints bonded with the Araldite® 2015, representative of longitudinal joints in a commercial aircraft fuselage skin. The CZM approach was validated against typical SLJ found in the literature [15, 22]. Different architectures were modelled, namely, a curved SLJ with free long edges, a SLJ with joggle detail, a wide curved SLJ with constrained long edges and a narrow and wide SLJ with initial damage. For the curvature effect, the study included three R (1000, 2000 and 3000 mm). The joggle design was implemented on the lower adherend in order to keep the adherends' axes collinear. The wide-curved SLJ, representative of an aircraft fuselage panel, was modelled with 2000 mm diameter and 500 mm width. The joggle architecture presented lower σ_y stresses and crack front strain energy release rate at the concave end of the overlap than the SLJ. Though, if the crack initiates in the joggle convex end, higher σ_y stresses and crack front strain energy release rate are found. Thus, in the joggle joints, the convex end is more susceptible to present adhesive failure than in conventional SLJ. In addition, the free edge approach in FEM studies proved to be important to predict the strength of real joints. The SLJ architecture with free edges (such as used for conventional test coupons) provides a conservative design to realistic joints with constrained edges. The

evaluation of initial damage effect showed that the small initial crack in a wide joint will propagate towards the two free edges to develop the same crack path as a narrow SLJ.

The mentioned studies mainly discussed the differences between curved joints and flat joints, but rare research has investigated the effect of geometric parameters on the curved joint behaviours. This work compares the performance of three adhesives (brittle, moderately ductile and ductile) in curved SLJ with CFRP adherends, considering the modification of the following geometric parameters: L_O, t_P and R. For the analysis of these joints, the FEM was used with CZM and included the internal stresses of the adhesive, joint strength and U. Before the numerical analysis, validation with experiments was carried out considering flat SLJ, with positive results. Thus, in this work, novel data is provided for curved CFRP SLJ, to assist in the design of curved structures.

2 Experimental details

2.1 Materials

The adherends were composed of unidirectional CFRP prepreg (SEAL® Texipreg HS 160 RM; Legnano, Italy), with 0.15 mm of ply thickness. The flat SLJ CFRP adherends were fabricated by hand lay-up of 20 plies along the joints' longitudinal direction, and then cured for 1 h at 130 °C and 2 bar of pressure in a hot-plates press. The fibre volume fraction for the mentioned curing conditions, including the pressure, temperature and ply thickness is 64%, as specified by the manufacturer. Under these conditions, the porosity content is negligible. Table 1 presents the elastic properties of a unidirectional lamina, modelled as elastic orthotropic in the FEM analysis [24].

Both validation and subsequent numerical study on the curved joints were undertaken using three adhesives: the epoxy Araldite® AV138 (brittle), the epoxy Araldite® 2015 (moderately ductile) and the polyurethane Sikaforce® 7888 (ductile). These adhesives were tested in previous works to obtain the estimated mechanical and fracture properties relevant for the application of the CZM technique [22, 25, 26], and they were selected because have been used widely in the aerospace and automotive commercial industries. Moreover, a wide range of material behaviours can be tested. The tensile mechanical properties were estimated by bulk tests, enabling the assessment of the Young's modulus (E), tensile yield stress (σ_{yie}), tensile strength (σ_f) and tensile failure strain (ε_f). The bulk specimens were manufactured following the NF T 76–142 French standard, to prevent the creation of voids. Typical tensile stress-tensile strain (σ-ε) curves of the adhesives tested in bulk are available in a former work [27]. The equivalent shear properties were estimated from Thick-Adherend Shear Tests (TAST) using steel adherends. The Double-Cantilever Beam (DCB) test was considered for G_{IC} and the End-Notched Flexure (ENF) test for G_{IIC}. All collected data is presented in Table 2.

Table 1 Elastic orthotropic properties of a unidirectional carbon-epoxy ply aligned in the fibres direction (x-direction; y and z are the transverse and through-thickness directions, respectively) [23]

E_x = 1.09E+05 MPa	ν_{xy} = 0.342	G_{xy} = 4315 MPa
E_y = 8819 MPa	ν_{xz} = 0.342	G_{xz} = 4315 MPa
E_z = 8819 MPa	ν_{yz} = 0.380	G_{yz} = 3200 MPa

2.2 Joint geometry

Figure 1 shows the geometry and dimensions of the flat SLJ (a), used for the CZM validation study, and curved SLJ (b), considered in the numerical parametric analysis. The joint dimensions are (expressed in mm): L_O = 10–80, width B = 15 (flat SLJ) or 25 (curved SLJ), length between grips L_T = 200, t_P = 2.4 (flat SLJ) or 1.2, 2.4 and 3.6 (curved SLJ), t_A = 0.2 and R = 1000, 2000 and 3000 (curved SLJ only). Eight different values of L_O were evaluated (10, 20, 30, 40, 50, 60, 70 and 80 mm).

2.3 Joint manufacturing and testing

Validation of the CZM technique for strength prediction was undertaken by the flat SLJ geometry (Fig. 1a). Initially, the CFRP plates with 300 × 300 mm^2 were manually stacked with the $[0]_{16}$ lay-up and cured in a hot-plates press. Following, adherends were cut with the proper dimensions. Surface preparation prior to bonding was accomplished by manual abrasion with fine mesh sandpaper and cleaning with acetone [28]. The joints were assembled and cured in a fabricated two-plate steel jig that assured the correct t_A by using a set of dummy blocks and 0.2 mm thick spacers. During this process, alignment tabs were also bonded at the specimens' ends for a correct load application during the tensile tests. After closing the upper jig plate, the set was kept under controlled humidity and temperature conditions for curing over a one-week period. As the final step towards testing, the excess adhesive at the overlap was trimmed in a milling machine to approximate the specimens to the theoretical shape depicted in Fig. 1(a) [29]. Finally, the tests were undertaken at room temperature in an electro-mechanical static testing machine (Shimadzu AG-X 100), at a displacement rate of 1 mm/min. The load data was acquired by a 100 kN load cell. The displacement of the grips holding the specimens was considered for the P-δ curves. For

Table 2 Properties of the adhesives Araldite® AV138, Araldite® 2015 and SikaForce® 7888 [22, 25, 26]

Property	AV138	2015	7888
Young's modulus, E [GPa]	4.89 ± 0.81	1.85 ± 0.21	1.89 ± 0.81
Poisson's ratio, ν	0.35 [a]	0.33 [a]	0.33 [a]
Tensile yield strength, σ_{yie} [MPa]	36.49 ± 2.47	12.63 ± 0.61	13.20 ± 4.83
Tensile failure strength, σ_f [MPa]	39.45 ± 3.18	21.63 ± 1.61	28.60 ± 2.0
Tensile failure strain, ε_f [%]	1.21 ± 0.10	4.77 ± 0.15	43.0 ± 0.6
Shear modulus, G [GPa]	1.56 ± 0.01	0.56 ± 0.21	0.71 [c]
Shear yield strength, τ_{yie} [MPa]	25.1 ± 0.33	14.6 ± 1.3	–
Shear failure strength, τ_f [MPa]	30.2 ± 0.40	17.9 ± 1.8	20 [a]
Shear failure strain, γ_f [%]	7.8 ± 0.7	43.9 ± 3.4	100 [a]
Toughness in tension, G_{IC} [N/mm]	0.20 [b]	0.43 ± 0.02	1.18 ± 0.22
Toughness in shear, G_{IIC} [N/mm]	0.38 [b]	4.70 ± 0.34	8.72 ± 1.22

[a] Manufacturer's data

[b] Estimated in reference [26], [c] estimated from Hooke's law

each value of L_O, five specimens were tested, with at least four valid results.

2.4 Numerical details

2.4.1 Model settings

Two-dimensional FEM analyses were performed in the software Abaqus®, evaluating the stress distributions and for CZM strength prediction. All analyses were carried out under the assumption of geometrical non-linearities, which was considered necessary to model the significant joint rotations and deformations of the SLJ. Two types of models were built. The models for the stress analysis used plane-strain quadrilateral elements (CPE4) in the adherends and in the adhesive layer, and stresses were captured at the mid-thickness of the adhesive. The models for the CZM analysis considered CPE4 elements for the adherends. For the adhesive, a single layer in the thickness direction of four-node cohesive elements (COH2D4) was considered. Equally, a CZM layer was inserted in both adherends between the 1st and 2nd plies closest to the adhesive, to emulate the interlaminar failure at this region, as it was observed in some experiments. A triangular traction-separation law was used for both materials. For the stress evaluation, a more refined mesh mainly in the adhesive layer was applied than the one used for the strength prediction, in order to obtain more precise results. The number of elements and bias ratio (i.e. mesh grading effects) largely depend on the need to obtain accurate stress estimations. Thus, the solid elements used for the adhesive layer in

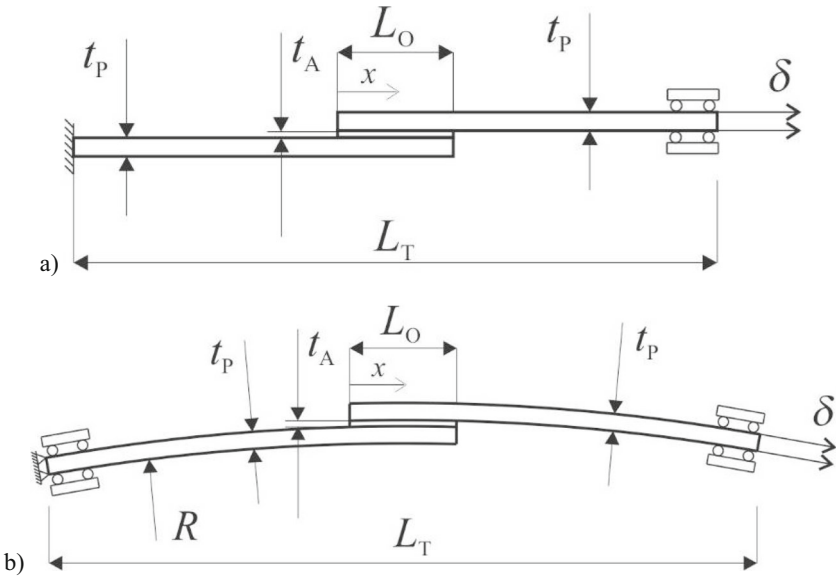

Fig. 1 Geometry and dimensions of the flat SLJ (**a**) and curved SLJ (**b**)

the thickness direction were ten times smaller than the ones used for strength analysis (i.e. side dimensions of 0.02 mm compared with 0.2 mm). Consequently, the overlap zone presented a higher mesh refinement. This mesh fine tuning was reduced towards the edges of the joint, although not affecting the accuracy of the results. Figure 2 shows a mesh example and overlap edge detail for a strength analysis model. To faithfully simulate the experimental setup, the boundary conditions for the flat SLJ were defined in a way that one of the joint edges was clamped and the other was subjected to a vertical restriction and a tensile displacement (Fig. 1a). On the other hand, for the curved lap joints, the direction of the applied displacement needs to be tangent to the axis of curvature of the substrate. To achieve this goal, a tensile displacement was applied perpendicularly to one of the edge butt faces of the model (Fig. 1b).

2.5 CZM formulation

CZM are based on relationships between stresses and relative displacements connecting homologous nodes of the cohesive elements, usually addressed as CZM laws. These laws simulate the elastic behaviour up to a peak load and subsequent softening, to model the gradual degradation of material properties up to complete failure. The areas under the traction-separation laws in tension or shear are equalled to G_{IC} or G_{IIC}, respectively. Under pure mode, damage propagation occurs at a specific integration point when the stresses are released in the respective traction-separation law. Under mixed mode, energetic criteria are often used to combine tension and shear [30]. In this work, triangular pure and mixed-mode laws, i.e. with linear softening, were considered. The elastic behaviour of the cohesive elements up to the tipping tractions is defined by an elastic constitutive matrix relating stresses and strains across the interface, containing E and the Poisson's coefficient (ν) as main parameters. Damage initiation under mixed-mode can be specified by different criteria. In this work, the quadratic nominal stress criterion was considered for the initiation of damage. After the cohesive strength in mixed-mode (t_m^0) is attained, the material stiffness is degraded. Complete separation is predicted by a linear power law form of the required energies for failure in the pure modes. For full details of the presented model, the reader can refer to reference [26]. The CZM properties of the adhesives for the simulations were taken from Table 2. The CZM laws for the interlaminar CFRP failure were obtained from a previous work using the same base material [25].

3 Results and discussion

3.1 Model validation

Validation of the CZM technique for static strength prediction is first performed using flat SLJ bonded with the three adhesives, for further application to the curved SLJ and respective parametric analysis.

3.1.1 Failure modes

This section details the flat SLJ failure modes. Experimentally, the specimens bonded with the Araldite® AV138, for $L_O = 10$ and 20 mm, presented a cohesive failure of the adhesive layer, while for L_O ranging from 30 to 80 mm, an interlaminar failure was observed along the full extent of the cohesive layer, with a small region of cohesive failure of the adhesive layer in some specimens. This different behaviour was associated to higher gradients of σ_y and τ_{xy} stresses for higher L_O, which triggered premature interlaminar for $L_O \geq 30$ mm. Figure 3(a) shows, as an example, the fracture surfaces of a specimen bonded with the Araldite® AV138 and $L_O = 40$ mm, in which it is clear the interlaminar failure and small spots of cohesive failure of the adhesive at the overlap edges.

The joints bonded with the Araldite® 2015 always presented a cohesive failure regardless of L_O, since both failure surfaces showed a thin adhesive layer (Fig. 3(b) shows the failed surfaces of a specimen with $L_O = 80$ mm). A cohesive failure was also found for the specimens bonded with the adhesive Sikaforce® 7888.

3.2 Joint strength

Fig. 4 shows the experimental and numerical P_m curves as function of L_O for the three studied adhesives. In addition, the experimental standard deviations were also included.

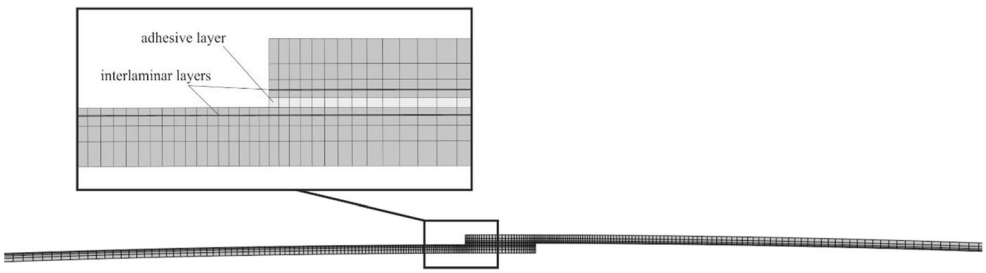

Fig. 2 Mesh example and overlap edge detail for a curved joint with $L_O = 10$ mm, $R = 2000$ mm and $t_P = 1.2$ mm (strength analysis)

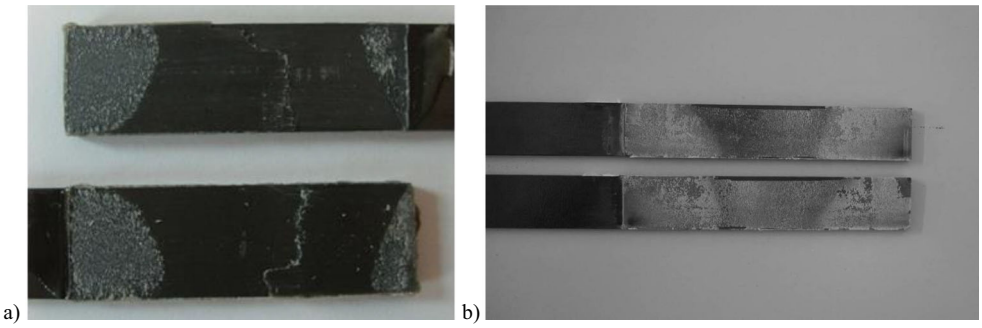

Fig. 3 Experimental interlaminar failure for a joint bonded with Araldite® AV138 and L_O = 40 mm (**a**) and cohesive failure of the adhesive for a joint bonded with the Araldite® 2015 and L_O = 80 mm (**b**)

It is notorious that P_m increases with L_O for all adhesives, in particular for the Sikaforce® 7888. In fact, increasing L_O from 10 to 80 mm origins a strength increment of 13.1, 16.6 and 25.8 kN, for the AV138, 2015 and 7888, respectively. For L_O = 10 mm, the Araldite® 2015 showed the lowest resistance (2.5 kN), whereas P_m for the Araldite® AV138 and Sikaforce® 7888 was higher by 18.3 and 85.3%, respectively. For L_O = 40 mm (representative example of an intermediate L_O) one can notice that the Araldite® AV138 presents the lowest P_m (8.8 kN). Actually, the Araldite® 2015 and the Sikaforce® 7888 resistance is higher by 5.9 and 97.3%, in the same order. For L_O = 80 mm, sharper differences were attained. The Araldite® AV138 continues to perform worst (16.0 kN), while the Araldite® 2015 and the Sikaforce® 7888 strength is higher by 19.3 and 90.4%, respectively. This behaviour occurs due the marked ductility of the Sikaforce® 7888. Actually, its inherent high degree of plasticity allows the joint to continuously withstand the loads until adhesive yielding is achieved in all bondline. On one hand, the brittle Araldite® AV138 fails soon after reaching its elastic limit, and thus it shows lower P_m by increasing L_O. On the other hand, the Araldite® 2015, which presents an intermediate degree of ductility, showed a slightly better performance than the Araldite® AV138 by increasing L_O.

Comparing the experimental and numerical data for the Araldite® AV138 depicted in Fig. 4(a), close results were found, especially for low L_O. Actually, the higher deviation was −9.1%, fond for L_O = 80 mm. Regarding the Araldite® 2015, whose results are shown in Fig. 4(b), the highest deviation was −7.0%, found for L_O = 70 mm. Higher deviations

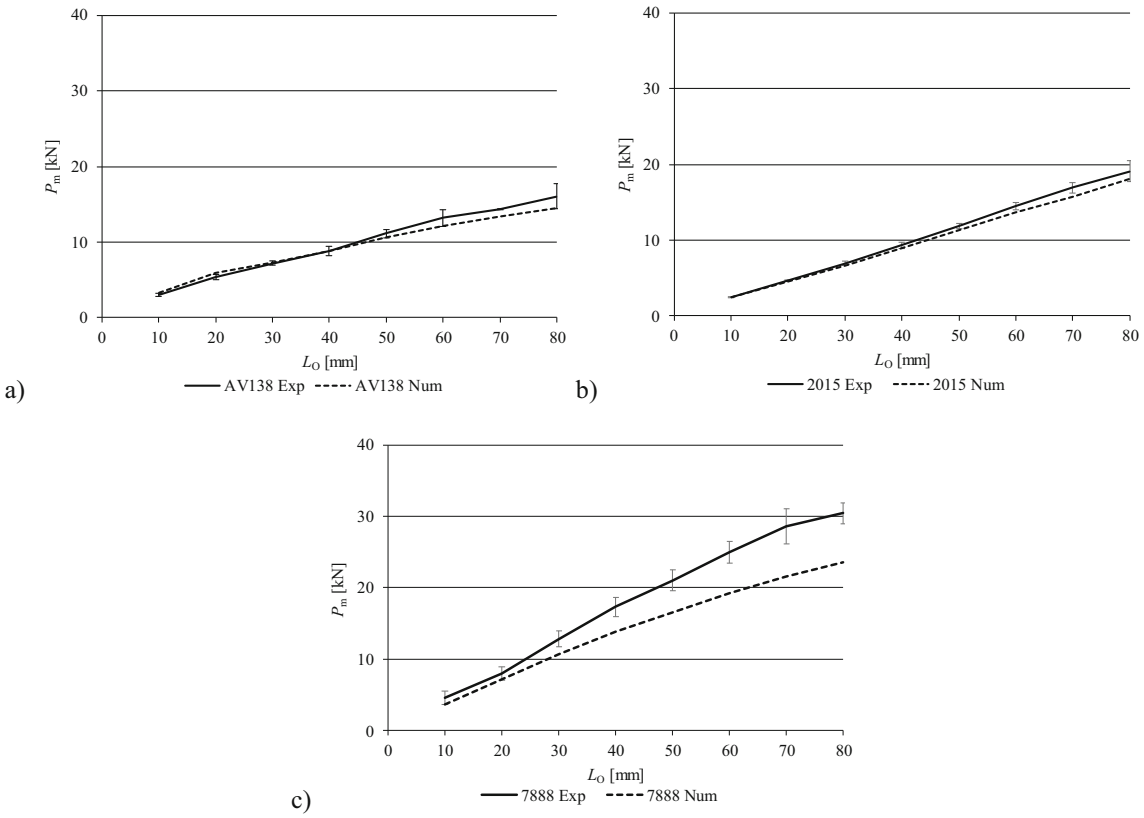

Fig. 4 Experimental and numerical P_m vs. L_O curves for the joints bonded with the Araldite® AV138 (**a**), Araldite® 2015 (**b**) and Sikaforce® 7888 (**c**).

were found in Fig. 4(c) for the adhesive Sikaforce® 7888. In fact, the lowest deviation for this adhesive was −10.0% found for $L_O = 20$ mm, while the higher deviation was −21.7% found for $L_O = 70$ mm. The main objective of the experimental tests in SLJ was to verify if the numerical method that will be applied in the parametric study of the curved joints constitutes a reliable approximation to real situations. Analysing the data of Fig. 4, one can stress that the chosen numerical methods were successful in the strength predicting of the JSS bonded with the Araldite® AV138 and 2015, despite a non-negligible difference for higher L_O. Oppositely, for the Sikaforce® 7888 a non-negligible discrepancy was found between the numerical and experimental results. Therefore, the triangular cohesive law used to simulate the adhesive's behaviour is not the most suitable for the Sikaforce® 7888, although it enables to achieve rough predictions. A solution to overcome these discrepancies is the use of a trapezoidal CZM law.

3.3 Parametric study of various curved joints

A purely numerical study is performed in this Section, after the validation presented in Section 4.1 regarding flat SLJ, to study the effect of different geometrical parameters on the performance of curved SLJ.

3.4 Stress analysis

In this stress analysis study, both σ_y and τ_{xy} stresses are normalized by the average shear stress registered along the adhesive layer (τ_{avg}) for the respective L_O. It should be mentioned that only one adhesive is analysed, due to the similarities of stress distributions between adhesives, in which the main difference is the increase of normalized peak stresses with the adhesive's stiffness. On account of the data of Table 2, the Araldite® AV138 clearly has the highest peak stresses and respective gradients.

Figure 5 relates to the t_P study. Figure 5(a) represents σ_y stresses along the adhesive layer for different values of L_O, considering the Araldite® 2015, $R = 2000$ mm, $L_O = 10$ mm and 80 mm, and all evaluated t_P. It is shown that σ_y stresses are essentially nil in the majority of the overlap, with a minor peak at $x/L_O \approx 0$ and major peak stresses approaching $x/L_O = 1$, which thus constitutes the critical location in which regards σ_y stresses and possible composite delaminations. This asymmetry counteracts the typical SLJ behaviour, in which σ_y stresses are symmetrical with respect to $x/L_O = 0.5$ [31, 32], and it arises due to the joints' curvature. For $L_O = 10$ mm, σ_y/τ_{avg} attained peaks of 6.83, 3.51 and 2.59 ($t_P = 1.2$, 2,4 and 3.6 mm, respectively), thus showing a drop of 62.1% between limit t_P. For $L_O = 80$ mm, maximum σ_y/τ_{avg} peak stresses of 27.73, 19.67 and 13.72 were found for increasing t_P between 1.2 and 3.6 mm (50.5% reduction between limit values). Thus, a clear σ_y reduction effect takes place by increasing t_P, which is caused by the higher joint stiffness promoted by bigger t_P, preventing localized peel deformations at the overlap ends. Actually, by increasing t_P, the induced curvature of the adherends is decreased, resulting in smaller σ_y stresses at the overlap edges, theoretically leading to an improved joint performance. Apart from this, increasing L_O tends to aggravate σ_y/τ_{avg} peak stresses by a large amount, although higher L_O cause the appearance of compressive σ_y stresses adjacent to the peel σ_y peak stresses. As the inner portion of the adhesive layer has practically no σ_y stresses, higher L_O tend to intensify the normalized σ_y/τ_{avg}. Figure 5(b) depicts τ_{xy} stresses in the adhesive layer the same L_O (10 and 80 mm) and all t_P, under fixed conditions (Araldite® 2015 and $R = 2000$ mm). The obtained stress plots also show that τ_{xy} stresses are much smaller in magnitude at the inner overlap (although not nil), peaking at both overlap edges. Due to the joint curvature, τ_{xy} peak stresses are more significant near to $x/L_O = 1$ rather than $x/L_O = 0$. As a result, it can be concluded that $x/L_O = 1$ is the stress critical location for both σ_y and τ_{xy} stresses, thus where damage is prone to initiate. Performing a comparison with flat SLJ, the typical stress symmetry is thus cancelled [31, 32]. The maximum τ_{xy}/τ_{avg} peak stresses for $L_O = 10$ mm were 4.45, 2.32 and 1.77 for increasing t_P between 1.2 to 3.6 mm (the

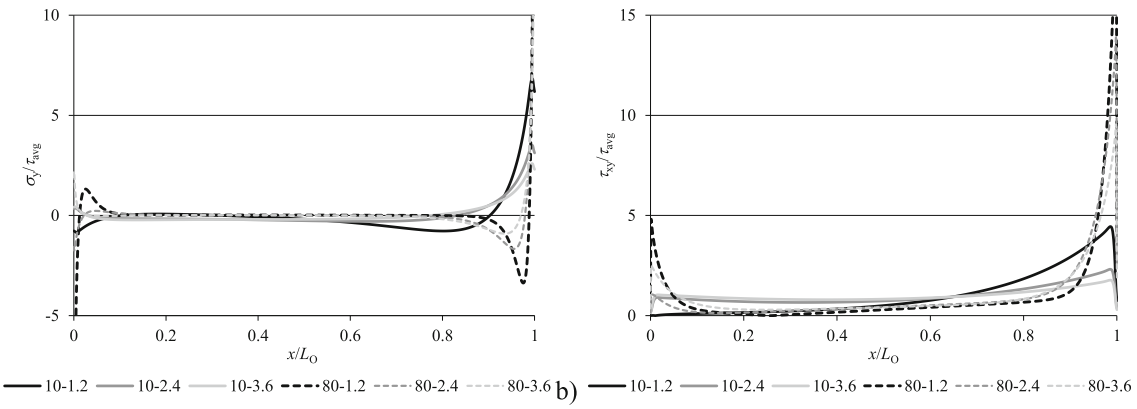

Fig. 5 Normalized σ_y (**a**) and τ_{xy} (**b**) stresses for the joints bonded with the Araldite® 2015, $R = 2000$ mm, $L_O = 10$ and 80 mm, and all evaluated t_P

reduction between limit values was 58.9%). Considering the joints with $L_O = 80$ mm, τ_{xy}/τ_{avg} peak stresses attained 19.93, 13.98 and 9.55 for $t_P = 1.2$, 2.4 and 3.6 mm, in this order (corresponding reduction of 52.1%). Similarly to σ_y stresses, higher t_P tend to reduce τ_{xy} peak stresses due to the increase of axial stiffening of the adherends, and consequent reduction of the shear-lag effect. This behaviour should be linked to higher joint strength as the normalized τ_{xy} peak stresses reduce. Oppositely, bigger L_O increase τ_{xy}/τ_{avg} peak stresses. In fact, higher L_O are naturally associated to a more pronounced shear-lag effect and more lightly stressed inner overlap, which overloads the overlap ends. Thus, despite the larger area to resist separation, τ_{xy} stresses distributions are more prone to localized failures.

Figure 6 pertains to the R study. Figure 6(a) shows σ_y/τ_{avg} stress distributions for fixed L_O and t_P (10 mm and 3.6 mm, respectively) and R between 1000 mm and 3000 mm. The previously described behaviour for σ_y stresses with fixed R at 2000 mm is valid for all tested R, i.e. with higher σ_y stress concentrations near to $x/L_O = 1$ than at the opposite overlap edge. The highest σ_y/τ_{avg} peak stresses were 3.60, 2.59 and 2.22 for $R = 1000$, 2000 and 3000 mm, respectively. These results indicate a reduction of σ_y peak stresses with the increase of R (percentile reduction of 28.3% between limit R). This variation takes place because of the progressive flattening of the adherends, which in a limit scenario would be perfectly flat (for $R = \infty$) and, in these conditions, σ_y stresses would be symmetric as it occurs in common SLJ. Thus, on account of σ_y stresses, bigger R should clearly benefit the joint strength. Figure 6(b) reports to τ_{xy}/τ_{avg} stresses for the same geometrical conditions. Here, an identical behaviour was found between all R, as it was found in the t_P study, with higher stress concentrations close to $x/L_O = 1$. For τ_{xy}/τ_{avg} stresses, the highest peak stresses at this location were 2.11, 1.77 and 1.64 for R between 1000 and 2000 mm, giving a maximum percentile reduction of 22.2%. The improved joint behaviour for larger R is also visible in this τ_{xy} stress analysis, being natural to achieve a symmetric stress distribution for $R = \infty$. It is thus confirmed that the bigger R is, the higher should the joint strength be.

3.5 Numerical failure modes

The failure modes are assessed by the variable SDEG, which represents the stiffness degradation of the cohesive elements and spans between 0 (undamaged cohesive elements) and 1 (failed cohesive elements). Although the scale itself is not presented, to simplify the figures, SDEG = 0 corresponds to light grey and SDEG = 1 to black, with the respective gradation between these two limits. The numerical failure modes were mostly identical individually for each adhesive. The joints bonded with the Araldite® AV138 essentially showed a concurrent interlaminar and cohesive failure of the adhesive layer, starting from $x/L_O = 1$ and propagating towards the other adhesive edge. Figure 7(a) shows the failure process for the joint with $t_P = 2.4$ mm and $L_O = 40$ mm, as an example. It is visible that failure grows simultaneously at the adhesive layer and between plies in the composite adherend. Only for two joint geometries ($L_O = 10$ mm and both $t_P = 2.4$ and 3.6 mm) the failure process was different: in these two geometries, failure was mostly interlaminar, starting at $x/L_O = 1$, and small or none damage in the adhesive layer (Fig. 7(b) shows failure for the joint with $L_O = 10$ mm and $t_P = 2.4$ mm). On the other hand, all joints bonded with the Araldite® 2015 and Sikaforce® 7888 experienced full cohesive failure of the adhesive layer, although with minor interlaminar damage. Figure 8 shows examples for the Araldite® 2015, $t_P = 2.4$ mm and $L_O = 20$ mm (a) and for the Sikaforce® 7888, $t_P = 2.4$ mm and $L_O = 60$ mm (b). The reported differences between adhesives are caused by caused by the higher magnitude of peak stresses for the Araldite® AV138, due to its higher stiffness, which triggers interlaminar failure of the composite. Oppositely, the smaller peak stresses and respective gradients for the other adhesives lead to minor interlaminar damage but no failure, while the adhesive layer undergoes broader degradation and failure.

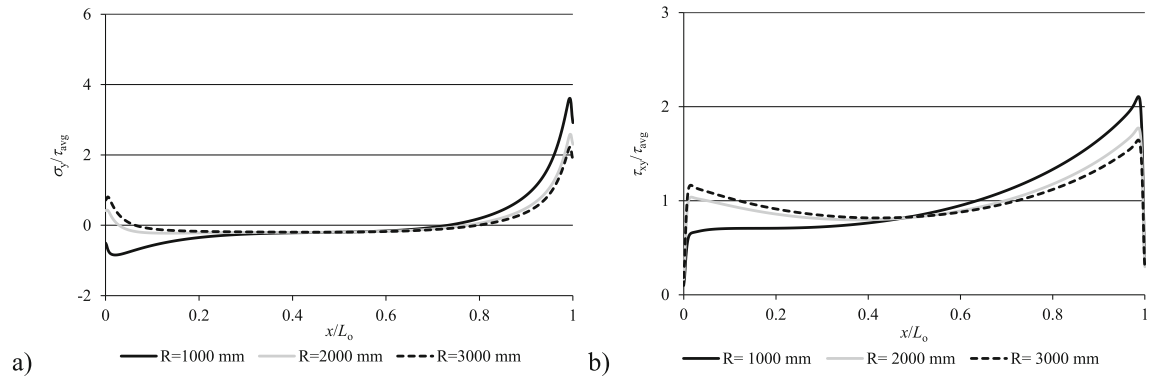

Fig. 6 Normalized σ_y (**a**) and τ_{xy} (**b**) stresses for the joints bonded with the Araldite® 2015, considering $R = 1000$, 2000 and 3000 mm, $L_O = 10$ mm and $t_P = 3.6$ mm

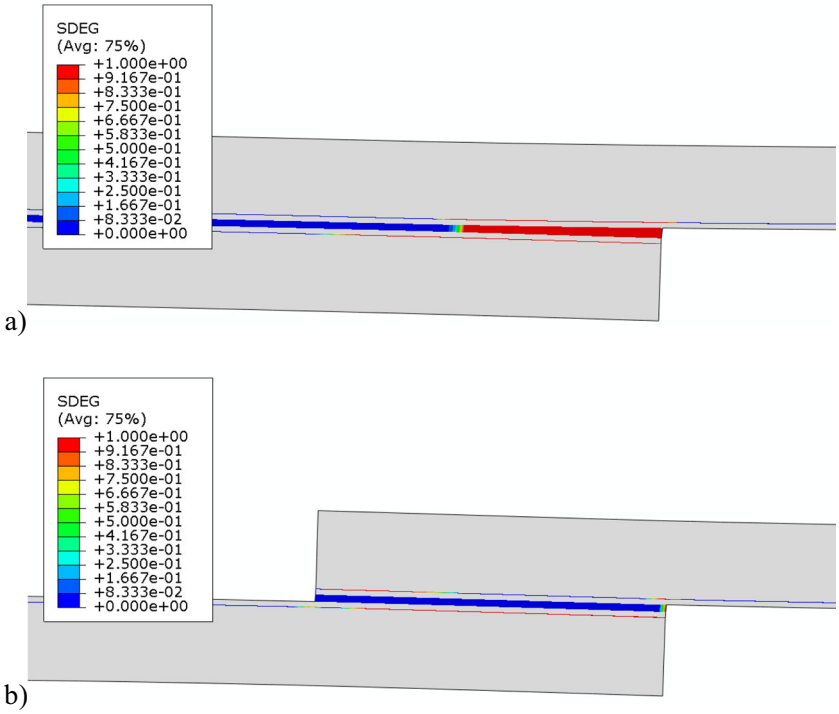

Fig. 7 Numerical concurrent and interlaminar failure for the joint bonded with Araldite® AV138, $t_P = 2.4$ mm and $L_O = 40$ mm (**a**) and interlaminar failure for the joint bonded with Araldite® AV138, $t_P = 2.4$ mm and $L_O = 10$ mm (**b**)

3.6 Strength prediction

Figure 9 represents the P_m vs. L_O curves for all adhesives considering $t_P = 1.2$ (a), 2.4 (b) and 3.6 mm (c) and a fixed R of 2000 mm.

Analysis of the results for $t_P = 1.2$ mm (Fig. 9a) shows a large discrepancy between adhesives. Actually, the Araldite® AV138 is much below the other two adhesives, despite its high strength. However, it is a brittle adhesive that cannot accommodate the peak stresses generated in the adhesive layer. As a result, P_m for this adhesive is below the Araldite® 2015 and Sikaforce® 7888 up to 73.4% and 78.4%, respectively, in both cases for $L_O = 80$ mm. The Araldite® 2015, despite being less strong than the Araldite® AV138, has moderate ductility

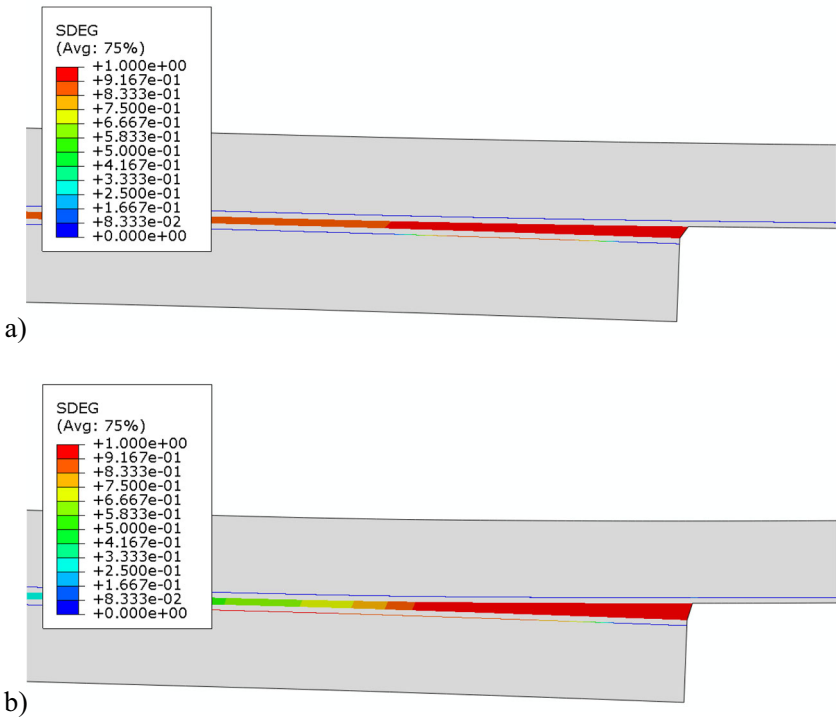

Fig. 8 Numerical cohesive failure of the adhesive for the joint bonded with Araldite® 2015, $t_P = 2.4$ mm and $L_O = 20$ mm (**a**) and bonded with the Sikaforce® 7888, $t_P = 2.4$ mm and $L_O = 60$ mm (**b**)

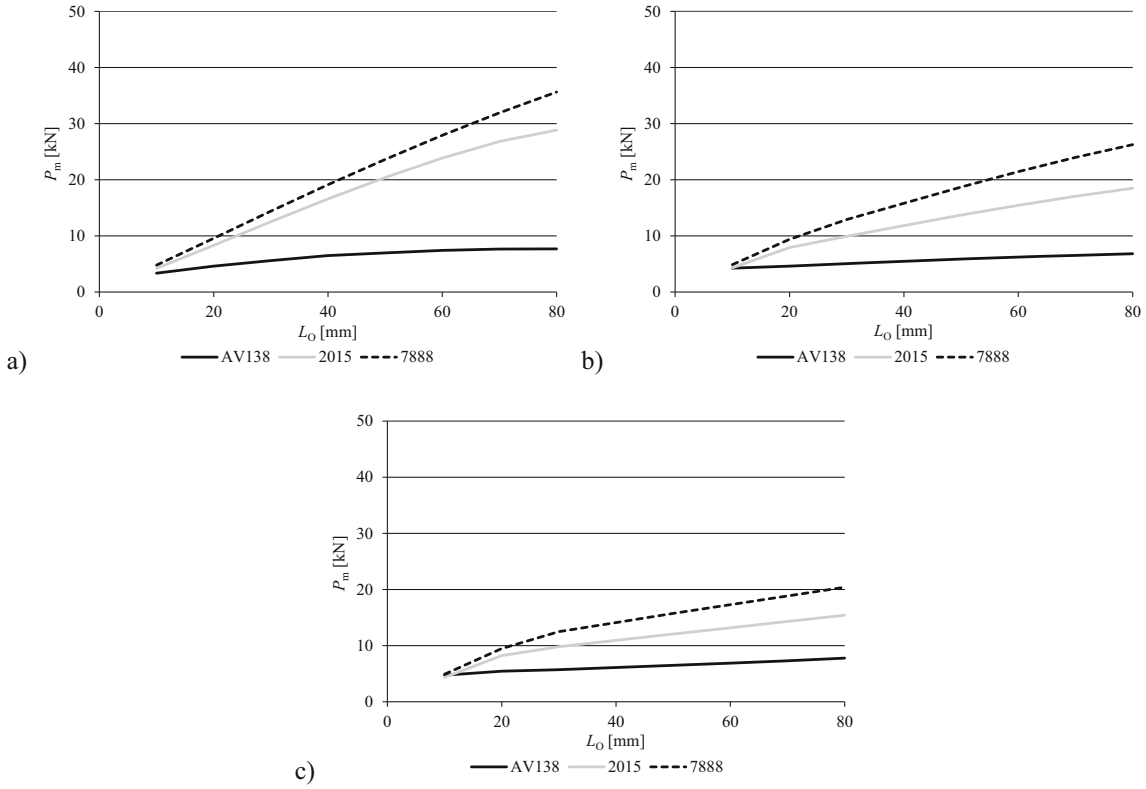

Fig. 9 P_m as a function of L_O for the joints bonded with the three adhesives and $t_P = 1.2$ (**a**), 2.4 (**b**) and 3.6 mm (**c**)

which, in the context of a bonded joint, gives it a significant advantage. The best results, disregarding L_O, were attained by the Sikaforce® 7888, since this polyurethane adhesive combines high strength and ductility. The maximum relative difference of this adhesive over the Araldite® 2015 was 23.4% for $L_O = 80$ mm. The P_m evolution with L_O is differing between adhesives. Between $L_O = 10$ and 80 mm, the percentile P_m improvement was 127.4% for the Araldite® AV138, 584.0% for the Araldite® 2015 and 641.1% for the Sikaforce® 7888. Thus, the Araldite® AV138 presented the worst results, which is intrinsically associated with its brittleness and increasing peak stresses with L_O. Actually, despite the increase in bonded area resisting separation, the adhesive cannot cope with the peak stresses and the joints end up by failing prematurely. On the other hand, ductile adhesives manage to absorb these peak stresses after yielding, keeping the overlap edges under loads while the inner overlap gets progressively loaded. As a result, τ_{avg} at failure is much higher than that when the limiting stresses of the adhesive are reached at the overlap edges. This occurs to a bigger extent for the Sikaforce® 7888 than for the Araldite® 2015, which justifies the practically linear P_m-L_O plot for the former adhesive.

The relative behaviour between adhesives is kept for both $t_P = 2.4$ mm (Fig. 9b) and $t_P = 3.6$ mm (Fig. 9c), although with different absolute magnitudes for P_m. Actually, between $t_P = 1.2$ and 2.4 mm for the Araldite® AV138, P_m slightly increased by 26.0% for $L_O = 10$ mm but then it reduced for all L_O up to 16.0% ($L_O = 50$ mm). A marginal P_m increase was also found for the Araldite® 2015 and Sikaforce® 7888 with $L_O = 10$ mm (2.5 and 1.6%, respectively), but then reductions were also found, especially for the bigger L_O (up to 36.4% for the Araldite® 2015 and $L_O = 70$ mm and 26.3% for the Sikaforce® 7888 and $L_O = 80$ mm). Comparing the joints with $t_P = 2.4$ and 3.6 mm, for the Araldite® AV138, a small P_m improvement was found for all L_O, up to 17.7% for $L_O = 20$ mm. For the other two adhesives, P_m marginally improved for the shortest L_O, but then it reduced by an increasing amount with L_O. The highest P_m reductions were 16.7% for the Araldite® 2015 and 22.3% for the Sikaforce® 7888, always for $L_O = 80$ mm. Thus, the typical behaviour, apart from few exceptions, consists of P_m reduction for higher t_P. This tendency somehow contradicts the stress analysis results in the elastic domain, especially for the ductile Araldite® 2015 and Sikaforce® 7888, in which both σ_y and τ_{xy} peak stresses diminish by increasing t_P. However, this effect can be explained by the curvature of the adherends, since their base geometry negatively affects the joints' overall ability of deforming themselves, which in turn induces premature failures. This effect is more prevalent for higher values of L_O.

Figure 10 represents the evolution of P_m with L_O between $R = 1000$, 2000 and 3000 mm, considering joints bonded with the Araldite® 2015 and $t_P = 2.4$ mm. The P_m evolution is similar between all R values, with a moderate increase with R, only varying the magnitude of P_m. Moreover, the P_m

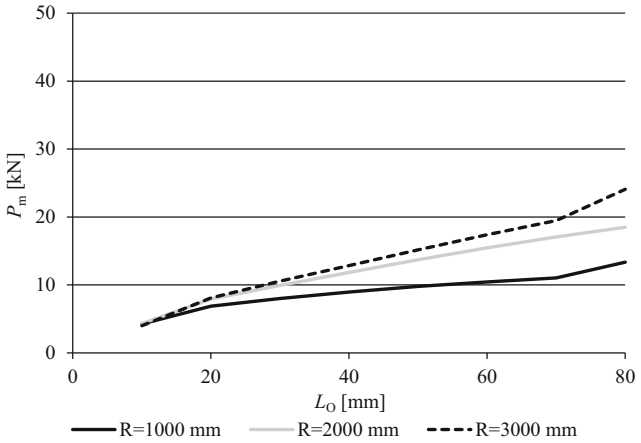

Fig. 10 P_m as function of L_O for the joints bonded with the Araldite® 2015 and $t_P = 2.4$ mm, considering different R

differences tend to be smaller or even almost nil for the smaller L_O and gradually increase with increasing L_O. Compared with the joints with $R = 2000$ mm, which is the base geometry, for $L_O = 10$ mm the relative differences were − 1.7% for $R =$ 1000 mm and + 7.7% for $R = 3000$ mm. For $L_O = 80$ mm, these differences increased to −27.9% ($R = 1000$ mm) and + 30.1% ($R = 3000$ mm). It is clear that the joints with the higher R have an improved performance, and this can be viewed as a consequence of more symmetrical stress distributions, as previously discussed. Actually, increasing R decreases the relative σ_y and τ_{xy} peak stresses at $x/L_O = 1$, whilst at the same time the less loaded edge at $x/L_O = 0$ becomes loaded, leading to a more efficient load transfer through the adhesive. Additionally, by increasing R, the induced deformation on the curved joints is less prevalent, which means that the joint is able to maintain a similar configuration to the traditional SLJ. In this manner the adhesive itself has a bigger margin to deform and resist more than the joints with the lower values of R.

3.7 Dissipated energy prediction

Figure 11 shows the values of U until failure as a function of L_O, considering $t_P = 1.2$ (a), 2.4 (b) and 3.6 mm (c) and a fixed R of 2000 mm. Each figure directly compares the three addressed adhesives. For $t_P = 1.2$ mm (Fig. 11a), large amounts of energy are dissipated for the Araldite® 2015 and Sikaforce® 7888, especially for large L_O, oppositely to the Araldite® AV138. For $L_O = 10$ mm, the values of $U = 0.53$, 1.10 and 2.08 J were registered by order of increasing ductility of the adhesives. Over this condition, the U improvements were 303.0%, 2228.0% and 1746.4%, in all cases attained for $L_O = 80$ mm. As the obtained results show, there are clear differences between the Araldite® AV138 and the Araldite® 2015 and Sikaforce® 7888, in line of what was previously observed in the P_m analysis. It is clear that the high stiffness

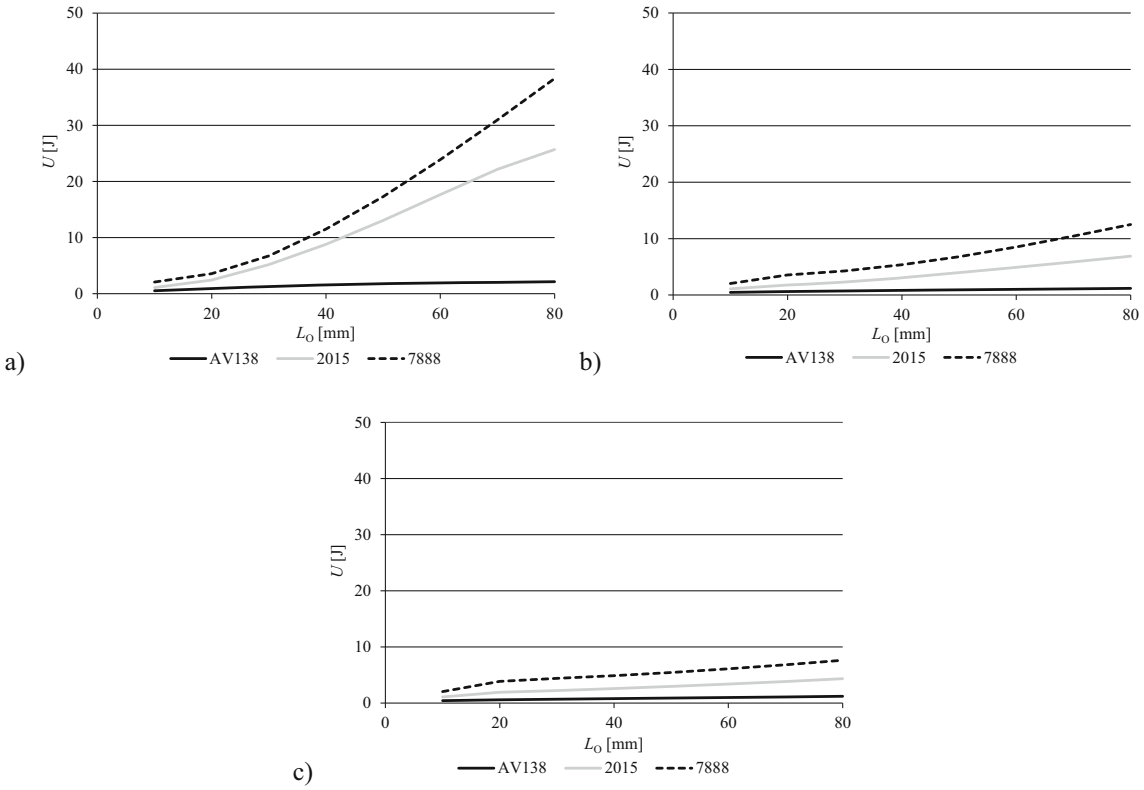

Fig. 11 U as function of L_O for the joints bonded with the three adhesives and $t_P = 1.2$ (**a**), 2.4 (**b**) and 3.6 mm (**c**)

and brittleness of the Araldite® AV138 negatively affects U, since this adhesive achieves failure very early in the tests due its low deformability. As a result, failure of the adhesive prevents the joint from storing U before failure and the measured U is much lower than for the other adhesives. On the other hand, the higher deformation capacity of the Sikaforce® 7888 allows it to store more energy during the tests than the Araldite® 2015 and, as a result, it presents the best results. Equally to the strength study, U tends to increase in direct proportion with L_O because of the higher P and failure displacements attained by the joints.

A significant t_P effect is also depicted in Fig. 11, by comparing the aforementioned results (a) with those of $t_P = 2.4$ (b) and 3.6 mm (c). Actually, U significantly reduced, but always keeping the U-increasing tendency with L_O. Over $t_P = 1.2$ mm, the joints with $t_P = 2.4$ mm showed a reduction in U that reached a maximum of 48.6% ($L_O = 50$ mm), 73.4% ($L_O = 70$ mm) and 67.4% ($L_O = 80$ mm) for the Araldite® AV138, Araldite® 2015 and Sikaforce® 7888, respectively. On the other hand, between $t_P = 2.4$ and 3.6 mm, the maximum percentile reductions were, by the same order of adhesives, 5.0% ($L_O = 10$ mm), 36.7% ($L_O = 80$ mm) and 39.0% ($L_O = 80$ mm). In both cases, the effect of L_O is also much smaller than for $t_P = 1.2$ mm. It is thus evident that, for joints with higher t_P (2.4 and 3.6), U tends to suffer a massive drop. This phenomenon ultimately means that the inner deformations on the adhesive layer are much smaller and, therefore, the value of U at the moment of the joint failure is very small for bigger t_P.

Figure 12 represents U in joints with $R = 1000$ mm, 2000 mm and 3000 mm, considering as fixed parameters the adhesive Araldite® 2015 and $t_P = 2.4$ mm. Following the aforementioned study, U increases steadily with L_O for all R. Between $L_O = 10$ and 80 mm, the percentile increases for this specific adhesive were 475.4%, 530.4% and 901.7% for $R =$ 1000, 2000 and 3000 mm, respectively. It is clear that the joints with large R have the best mechanical performance, as

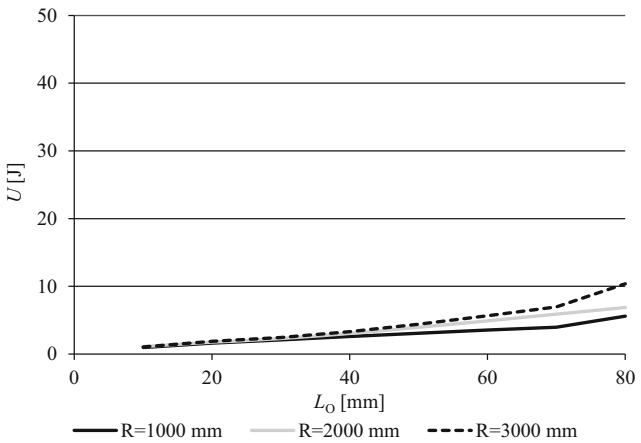

Fig. 12 U as function of L_O for the joints bonded with the Araldite® 2015 and $t_P = 2.4$ mm, considering different R

shown by the higher U. Moreover, this difference enlarges by increasing L_O. Over $R = 1000$ mm, the U performance improvements reached 48.1% for $R = 2000$ mm ($L_O = 70$ mm) and 85.7% for $R = 3000$ mm ($L_O = 80$ mm). This is due to the fact that higher R tend to turn stresses symmetric (Fig. 6), thus removing the large discrepancy in the σ_y and τ_{xy} stress distributions that triggers premature failures. As depicted in Fig. 10, this modification increases P_m, which causes an improved energy absorption to failure.

4 Conclusions

The present work aimed to experimentally and numerically compare the tensile behaviour of curved CFRP joints bonded with three adhesives, considering the variation of three geometrical parameters that highly impact the joints' performance: L_O, t_P and R. Former joint validation was undertaken with the same adhesives, considering flat, i.e. $R = \infty$ joints. The validation study, by considering only the variation of L_O, showed a strong dependence on P_m by this variable and a major difference between adhesives. The CZM technique, by employing a triangular-based cohesive law, showed accurate P_m predictions for the brittle and moderately ductile adhesives, but P_m under predictions for the ductile adhesive. However, this CZM formulation was chosen due to ease of application and ready application in commercial software. The parametric CZM study that followed based the analysis on elastic stress distributions, which were used to enable a detailed discussion on the joints' performance with the aforementioned tested parameters and on P_m and U. The stress analysis revealed a major σ_y and τ_{xy} peak stresses' asymmetry induced by the adherends' curvature, which would be responsible for smaller P_m and U performance with lower R. On the other hand, peak stresses highly increased with L_O, as expected by the existing literature data for flat joints, and they reduced by increasing t_P. The P_m comparison showed major improvements with L_O for the moderately ductile and ductile adhesives and smaller differences for the brittle adhesive. Between adhesives, the ductile adhesive performed best and the brittle worst. Opposing to the expected by a purely elastic stress analysis, t_P negatively affected P_m by a significant amount. Increasing R tends to provide higher P_m, as the joints approach the flat SLJ geometry. The tendency of U followed that of P_m, with a major reduction for higher t_P, although increasing with P_m due to the higher transmitted loads.

As a result of this work, it can be concluded that large curvatures ($R \leq 2000$ mm) have a significant effect on the stress distribution and load capacity of the joint, while the traditional method of using laboratory flat joints to predict the curved joints' behaviour will predict in less-conservative results. It can be also suggested that, for realistic joint applications with curved geometries, moderately ductile and

ductile adhesives would be more beneficial as their high degree of plasticity could support a larger joint deformation and withstand the loads until adhesive yielding. Based on the above observations, material and geometrical guidelines on the design of curved bonded joints were provided.

Authors' contributions J.M.C. Correia carried out the numerical analysis and respective data analysis, R.D.S.G. Campilho and R.J.B. Rocha performed the validation study and sketched the paper. Y. Liu and L.D.C. Ramalho built and revised the paper until final form.

Funding This work received no funding.

Data availability The raw/processed data required to reproduce these findings cannot be shared at this time due to technical or time limitations.

Compliance with ethical standards

Conflict of interest The authors declare that they have no conflict of interest.

Code availability Not applicable.

References

1. Tenney DR, Davis Jr JG, Pipes RB, Johnston N (2009) NASA composite materials development: lessons learned and future challenges. Paper presented at the NATO RTO AVT-164 workshop on support of composite systems, Bonn, Germany
2. Adams RD, Comyn J, Wake WC (1997) Structural adhesive joints in engineering, 2nd edn. Chapman & Hall, London
3. Valenza A, Fiore V, Fratini L (2011) Mechanical behaviour and failure modes of metal to composite adhesive joints for nautical applications. Int J Adv Manuf Technol 53(5):593–600. https://doi.org/10.1007/s00170-010-2866-1
4. Kinloch AJ (1987) Adhesion and adhesives: science and technology. Springer, Heidelberg
5. Peng D, Liu Q, Li G, Cui J (2019) Investigation on hybrid joining of aluminum alloy sheets: magnetic pulse weld bonding. Int J Adv Manuf Technol 104(9):4255–4264. https://doi.org/10.1007/s00170-019-04215-x
6. Petrie EW (1999) Handbook of adhesives and sealants, 2nd edn. McGraw-hill, New York
7. Alfano G (2006) On the influence of the shape of the interface law on the application of cohesive-zone models. Compos Sci Technol 66(6):723–730. https://doi.org/10.1016/j.compscitech.2004.12.024
8. Barenblatt GI (1959) The formation of equilibrium cracks during brittle fracture. General ideas and hypotheses. Axially-symmetric cracks. J Appl Math Mech 23(3):622–636. https://doi.org/10.1016/0021-8928(59)90157-1
9. Dugdale DS (1960) Yielding of steel sheets containing slits. J Mech Phys Solids 8(2):100–104. https://doi.org/10.1016/0022-5096(60)90013-2
10. Elices M, Guinea GV, Gómez J, Planas J (2002) The cohesive zone model: advantages, limitations and challenges. Eng Fract Mech 69(2):137–163. https://doi.org/10.1016/S0013-7944(01)00083-2
11. da Silva LFM, Campilho RDSG (2012) Advances in numerical modelling of adhesive joints. In: Advances in Numerical Modeling of Adhesive Joints. Springer Berlin Heidelberg, pp 1–93. doi:citeulike-article-id:11791960. https://doi.org/10.1007/978-3-642-23608-2_1
12. Ojalvo IU, Eidinoff HL (1978) Bond thickness effects upon stresses in single-lap adhesive joints. AIAA J 16(3):204–211. https://doi.org/10.2514/3.60878
13. Adams R, Atkins R, Harris J, Kinloch A (1986) Stress analysis and failure properties of carbon-fibre-reinforced-plastic/steel double-lap joints. J Adhes 20(1):29–53
14. Liao L, Huang C, Sawa T (2013) Effect of adhesive thickness, adhesive type and scarf angle on the mechanical properties of scarf adhesive joints. Int J Solids Struct 50(25):4333–4340. https://doi.org/10.1016/j.ijsolstr.2013.09.005
15. Taib AA, Boukhili R, Achiou S, Boukehili H (2006) Bonded joints with composite adherends. Part II Finite element analysis of joggle lap joints. Int J Adhes Adhes 26(4):237–248. https://doi.org/10.1016/j.ijadhadh.2005.03.014
16. Liu Y, Lemanski S, Zhang X (2018) Parametric study of size, curvature and free edge effects on the predicted strength of bonded composite joints. Compos Struct 202:364–373. https://doi.org/10.1016/j.compstruct.2018.02.017
17. Ascione F, Mancusi G (2012) Curve adhesive joints. Compos Struct 94(8):2657–2664. https://doi.org/10.1016/j.compstruct.2012.03.024
18. Temiz Ş, Akpinar S, Aydın MD, Sancaktar E (2013) Increasing single-lap joint strength by adherend curvature-induced residual stresses. J Adhes Sci Technol 27(3):244–251. https://doi.org/10.1080/01694243.2012.705509
19. Parida SK, Pradhan AK (2014) Influence of curvature geometry of laminated FRP composite panels on delamination damage in adhesively bonded lap shear joints. Int J Adhes Adhes 54:57–66. https://doi.org/10.1016/j.ijadhadh.2014.05.003
20. Sato C (2011) Stress estimation of joints having adherends with different curvatures bonded with viscoelastic adhesives. Int J Adhes Adhes 31(5):315–321. https://doi.org/10.1016/j.ijadhadh.2011.01.007
21. Dillard DA (1988) Stresses between Adherends with different curvatures. J Adhes 26(1):59–69. https://doi.org/10.1080/00218468808071274
22. Campilho RDSG, Banea MD, Neto JABP, da Silva LFM (2013) Modelling adhesive joints with cohesive zone models: effect of the cohesive law shape of the adhesive layer. Int J Adhes Adhes 44:48–56. https://doi.org/10.1016/j.ijadhadh.2013.02.006
23. Oliveira JJG, Campilho RDSG, Silva FJG, Marques EAS, Machado JJM, da Silva LFM (2020) Adhesive thickness effects on the mixed-mode fracture toughness of bonded joints. J Adhes 96(1–4):300–320. https://doi.org/10.1080/00218464.2019.1681269
24. Campilho RDSG, de Moura MFSF, Domingues JJMS (2005) Modelling single and double-lap repairs on composite materials. Compos Sci Technol 65(13):1948–1958. https://doi.org/10.1016/j.compscitech.2005.04.007
25. Neto JABP, Campilho RDSG, da Silva LFM (2012) Parametric study of adhesive joints with composites. Int J Adhes Adhes 37(0):96–101. https://doi.org/10.1016/j.ijadhadh.2012.01.019
26. Campilho RDSG, Banea MD, Pinto AMG, da Silva LFM, de Jesus AMP (2011) Strength prediction of single- and double-lap joints by standard and extended finite element modelling. Int J Adhes Adhes 31(5):363–372. https://doi.org/10.1016/j.ijadhadh.2010.09.008
27. Nunes SLS, Campilho RDSG, da Silva FJG, de Sousa CCRG, Fernandes TAB, Banea MD, da Silva LFM (2016) Comparative failure assessment of single and double-lap joints with varying adhesive systems. J Adhes 92:610–634. https://doi.org/10.1080/00218464.2015.1103227
28. Wang S, Liang W, Duan L, Li G, Cui J (2020) Effects of loading rates on mechanical property and failure behavior of single-lap adhesive joints with carbon fiber reinforced plastics and aluminum

alloys. Int J Adv Manuf Technol 106(5):2569–2581. https://doi.org/10.1007/s00170-019-04804-w

29. Pizzorni M, Lertora E, Gambaro C, Mandolfino C, Salerno M, Prato M (2019) Low-pressure plasma treatment of CFRP substrates for epoxy-adhesive bonding: an investigation of the effect of various process gases. Int J Adv Manuf Technol 102(9):3021–3035. https://doi.org/10.1007/s00170-019-03350-9
30. Kim K (2015) Softening behaviour modelling of aluminium alloy 6082 using a non-linear cohesive zone law. P I Mech Eng L-J Mat 229 (5):431–435. https://doi.org/10.1177/1464420714525134
31. Ye J, Yan Y, Li J, Hong Y, Tian Z (2018) 3D explicit finite element analysis of tensile failure behavior in adhesive-bonded composite single-lap joints. Compos Struct 201:261–275. https://doi.org/10.1016/j.compstruct.2018.05.134
32. Jiang W, Qiao P (2015) An improved four-parameter model with consideration of Poisson's effect on stress analysis of adhesive joints. Eng Struct 88:203–215. https://doi.org/10.1016/j.engstruct.2015.01.027